Extraction and Visual Analysis of Potential Vorticity Banners around the Alps

Robin Bader, Michael Sprenger, Nikolina Ban, Stefan Rüdisühli, Christoph Schär and Tobias Günther

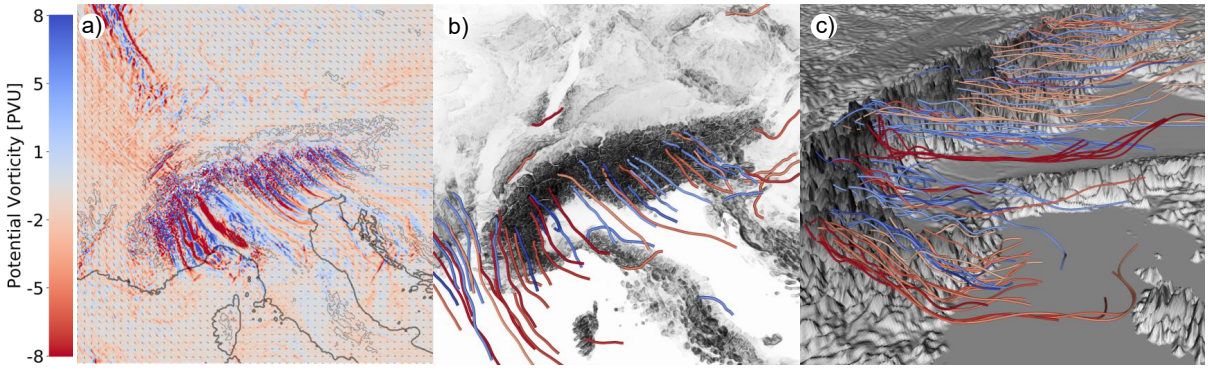

Fig. 1. Potential vorticity (PV) banners are created during the detachment of flow from the mountain topography and can extend several hundred kilometers downstream. Here, the banners appear in the lee of the Alps as line-shaped regions with significantly negative (blue) or positive (red) PV values. **(a)** Traditional visualization of potential vorticity as 2D slice, computed at a fixed altitude level. **(b)** Our method robustly extracts PV banners that originate from flow detachment at the topography and removes visual clutter. **(c)** Visualization of our PV banner lines in 3D before clustering into banner representatives. Our method allows for the interpretation of the spatial extent of the banners and shows PV banners across all altitude levels.

Abstract—Potential vorticity is among the most important scalar quantities in atmospheric dynamics. For instance, potential vorticity plays a key role in particularly strong wind peaks in extratropical cyclones and it is able to explain the occurrence of frontal rain bands. Potential vorticity combines the key quantities of atmospheric dynamics, namely rotation and stratification. Under suitable wind conditions elongated banners of potential vorticity appear in the lee of mountains. Their role in atmospheric dynamics has recently raised considerable interest in the meteorological community for instance due to their influence in aviation wind hazards and maritime transport. In order to support meteorologists and climatologists in the analysis of these structures, we developed an extraction algorithm and a visual exploration framework consisting of multiple linked views. For the extraction we apply a predictor-corrector algorithm that follows streamlines and realigns them with extremal lines of potential vorticity. Using the agglomerative hierarchical clustering algorithm, we group banners from different sources based on their proximity. To visually analyze the time-dependent banner geometry, we provide interactive overviews and enable the query for detail on demand, including the analysis of different time steps, potentially correlated scalar quantities, and the wind vector field. In particular, we study the relationship between relative humidity and the banners for their potential in indicating the development of precipitation. Working with our method, the collaborating meteorologists gained a deeper understanding of the three-dimensional processes, which may spur follow-up research in the future.

Index Terms—Scientific Visualization, potential vorticity, meteorology, feature extraction.

1 Introduction

Many meteorological processes, such as the formation of clouds and precipitation, are inherently three-dimensional and exhibit a high temporal and spatial variability. Meteorologists are required to understand these processes since they are not only crucial for short-term numerical weather prediction, but also for long-term climate change simulations. Because of the high spatial and temporal resolution required to resolve these processes with adequate accuracy, the analysis of meteorological data becomes more and more challenging [28, 37, 38]. Within the continuous basic meteorological fields (e.g., wind speed or temperature) distinct meteorological features are embedded and can be identified. In fact, it is one goal of synoptic meteorology[1] to identify these key drivers of the weather evolution and their potential interaction. For instance, at a synoptic-scale, well-known Eulerian features are extratropical cyclones[2] and jet streams, and an example for a Lagrangian feature is the warm-conveyor belt [44]. In this paper, we focus on a less familiar mesoscale feature, namely on so-called potential vorticity (PV) banners in the lee of the European Alps. The existence of PV banners has initially been proposed based on numerical experiments [1] and has later been confirmed in field experiments using multiple research aircrafts [7, 39]. Indeed, when the synoptic-scale wind turns into a direction crossing the Alpine ridge, low-level elongated bands of potential vorticity form [1, 5]. These so-called PV banners are represented by pairs of banners with anomalously positive and negative values and can be attributed to flow splitting, either on the scale of the whole Alps (primary banners), or on that of individual massifs and mountain peaks (secondary banners). Fig. 1 displays a conventional 2D slice (a) of potential vorticity in the atmosphere above the Alps and our interactive visualization of the extracted 3D PV banners (b, c).

Due to the high resolution of the numerical weather prediction (NWP) data and the additional temporal dimension [34], an effective visual analysis of the dynamic behavior of PV banners is a challenging problem. PV banners are intrinsically three-dimensional structures and their sometimes short-lived presence depends on a number of factors.

- *Robin Bader and Tobias Günther are with the Dep. of Computer Science, ETH Zürich. E-mail: baderr@student.ethz.ch, tobias.guenther@inf.ethz.ch.*
- *Michael Sprenger, Nikolina Ban, Stefan Rüdisühli and Christoph Schär are with the Institute for Atmospheric and Climate Science, ETH Zürich. E-mail: michael.sprenger/nikolina.ban/stefan.ruedisuehli/schaer@env.ethz.ch.*

[1] Synoptic meteorology considers processes on the 1000 km scale.

[2] Extratropical cyclones appear north and south of 30 degrees latitude.

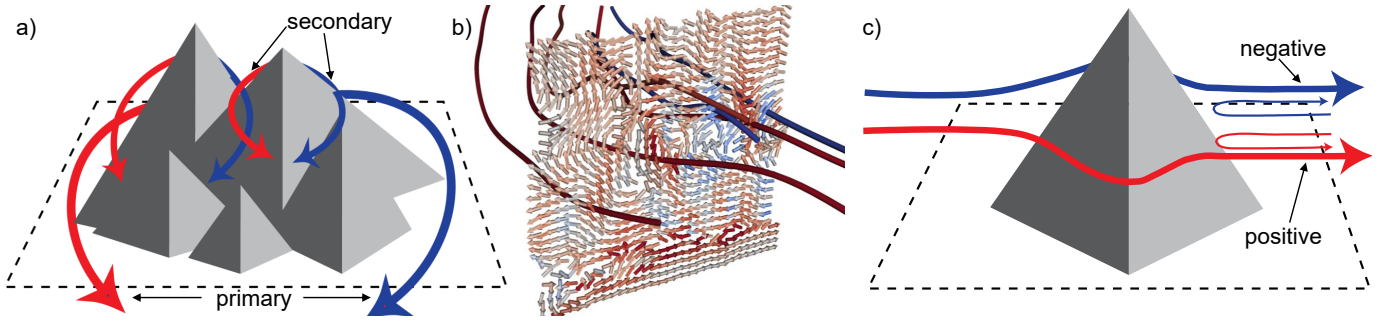

Fig. 2. **(a)** PV banners form in the lee of a mountain when air flows around rather than over it. Primary banners, colored in red (positive PV) and blue (negative PV), are on the scale of the whole mountain. Their width is determined by boundary layer processes and turbulence. The width of secondary banners, which are created in the lee of individual peaks and massifs, is determined by the upstream topography. **(b)** Vertical cross section of secondary banners in a numerically-simulated flow, showing the velocity using an arrow plot projected onto a plane. The color denotes the PV value at each point and the arrows highlight the swirling motion. **(c)** The rotation direction of a potential vorticity banner depends on which side the air flows around the mountain.

Understanding their creation and evolution is a multi-field visualization problem, since the presence of banners is linked to other meteorological attributes. The cores of PV banners are temporally moving and deforming, multiple PV banners may be in a very close proximity, and the numerical data is highly anisotropic. To facilitate further meteorological research on PV banners and to improve the comprehension of their underlying complex three-dimensional meteorological processes, we collaborated closely with four domain scientists. Together, we devised an automatic feature extraction approach that computes a geometric line representation for each banner. From the geometric representation, we extract curve characteristics (length, curvature, life time etc.), which can be interactively explored alongside given meteorological attributes (e.g., relative humidity, temperature, or precipitation) in order to study correlations. Our system consists of three components:

- **Feature Extraction:** We develop an automatic predictor-corrector algorithm that places seed points on the mountains and uses the wind vector field and the potential vorticity's gradient to extract the core lines of minimal and maximal potential vorticity.
- **Clustering:** We use agglomerative hierarchical clustering to remove duplicate PV core lines. This enables the observation of their temporal life cycle and allows us to distinguish their origins.
- **Visualization:** We provide multiple linked views that display the spatial embedding in 3D and the time-dependent evolution of properties along the curves. Our user interface provides a flexible node-based editor with interactive filtering, linking, and brushing.

We extract and visualize the PV banners in two high-resolution numerical simulations, and we demonstrate the effectiveness of the visualization system in explaining the inherently three-dimensional processes of PV creation and evolution, and their relationship with meteorological attributes. In particular, we identify two phenomena that our domain scientists were interested in and are intractable to comprehend from conventional 2D slices: cross flows of PV banners in different altitudes and the vertical waviness of PV banners.

2 Background and Related Work

2.1 Definition of Potential Vorticity

Potential vorticity is a signed scalar value that is derived from vorticity, describing the rotation of an air parcel[3] between levels of constant potential temperature. An air parcel's PV is conserved during advection and can only change due to diabatic heating[4] or friction [14, 22]. PV is invariant to an air parcel's change in position and altitude, it therefore behaves under adiabatic and frictionless conditions as a tracer, i.e., it is advected along by the ambient flow field. Note, however, that PV is not passively advected by the wind, as for instance dye introduced in water. Rather, by means of the invertibility principle, PV is able to influence the ambient flow field itself [22]. This behavior as an active, in contrast to a passive tracer, leads to fascinating meteorological features, of which Diabatic Rossby Waves are one specific example [6].

Potential vorticity Q is proportional to the dot product of the absolute vorticity vector and the three-dimensional gradient of potential temperature. The absolute vorticity ζ_a is computed from the air velocity $\mathbf{v}$ defined relative to a coordinate frame rotating with the Earth. Therefore, it includes the Coriolis parameter $f = 2\Omega\sin(\varphi)$ applied to the unit vector $\mathbf{k}$ in vertical direction, where $\Omega = 7.29 \cdot 10^{-5}$ rad/s is the angular velocity of the Earth, and φ denotes the latitude:

$$\zeta_a = \nabla \times \mathbf{v} + f \cdot \mathbf{k} \tag{1}$$

The absolute vorticity of an air parcel will change if it is stretched (or compressed) in the vertical direction, but the potential vorticity is conserved in adiabatic and inviscid flows.

The potential temperature θ of an air parcel at pressure p is the temperature that the parcel would attain if adiabatically brought to a standard reference pressure p_0. It is given by

$$\theta = T\left(\frac{p_0}{p}\right)^{R/c_p} \tag{2}$$

where T, R, c_p are the temperature, gas constants, and specific heat capacity at constant pressure, respectively. The ratio $R/c_p = 0.286$ is a constant for dry air. Finally, the potential vorticity Q is defined following Ertel [14] as:

$$Q = \frac{\zeta_a \cdot \nabla\theta}{\rho} \tag{3}$$

where ρ is the density of the air parcel and Q is denoted by potential vorticity units (PVU) which are defined as 1 PVU $= \frac{10^{-6} \cdot K \cdot m^2}{kg \cdot s}$.

2.2 Potential Vorticity Banners

When synoptic-scale wind turns into a direction crossing the Alpine ridge, low-level elongated bands of potential vorticity form [1,5]. These so-called PV banners are represented as structures with low or high PV value and can be attributed to flow splitting. They can be categorized into primary banners (on the scale of the whole Alps) or secondary banners (individual massifs and mountain peaks) as schematically visualized in Fig. 2a. The primary PV banners are jointly responsible for the development of cyclones in the lee of the Alps, see e.g., Kljun et al. [26] and references therein. In secondary PV banners, an inertial (or symmetric) instability is released in the negative PV banner [21]. Negative PV (and symmetric instability) is assumed to play a key role in particularly strong wind peaks embedded in extratropical cyclones.

[3] An air parcel is a finite-sized package of air.

[4] Diabatic heating is either associated with a thermodynamic heat exchange with the surrounding (e.g. by radiation) or by latent heat release due to phase changes of water and ice (e.g. in cloud droplet formation). Adiabatic heating and cooling is associated with an air parcel's compression and expansion.

It was also hypothesized that the symmetric instability is able to explain the occurrence of elongated rain bands [4] – an idea that was recently further discussed by Schumacher et al. [41] for convective snow bands downstream of the Rocky Mountains and by Siedersleben and Gohm [43] for Alpine flows. In order to follow up on these meteorological questions, we use our visualizations to investigate in two cases whether the presence of PV banners can influence precipitation by studying the correlation with relative humidity.

Air parcels within PV banners rotate around a vertical axis along the common banner's core line, which may be straight or curved. Fig. 2b shows the vertical velocity profile which highlights the swirling motion around the core line. The rotation direction depends on which side the air flows around the peak, as illustrated in Fig. 2c. The banners encompass the wake of the topographic obstacle (i.e., a region of decelerated flow), either on the scale of the whole obstacle (primary banners) or of individual massifs and peaks (secondary banners).

2.3 Feature Line Extraction

Extracting the extremal lines of potential vorticity as geometric representation of the banner center is particularly useful because it removes visual occlusion and clutter, provides a concise picture of the structure of PV banners, and it enables the observation of the dynamics of meteorological processes along the lines.

Extremal lines are features of a 3D scalar field along which the scalar function becomes minimal or maximal with respect to a local neighborhood [13]. The extraction of extremal lines has been subject to a large body of research (see Kindlmann et al. [25]) and found numerous applications (see Kern et al. [24]) in the extraction of jet-stream core lines, in the extraction of vortex core lines using maximum lines of Q-criterion [35], minimum lines of pressure [29], or maximum lines of vorticity magnitude [46]. Peikert and Roth [31] introduced the parallel vectors operator and showed that many of the above feature line definitions can be expressed as the union of points at which two vector fields are parallel.

Extremal line extraction algorithms can be categorized into local and integration-based methods. Local methods subdivide the domain into cells, solve for parallel vector points on each cell boundary independently and finally connect the results [17, 19].

Banks and Singer [3] presented a predictor-corrector method to find vortex core lines, which forms the basis of our extraction algorithm. This integration-based method is more robust in avoiding typically spurious results induced by local methods.

The predictor-corrector algorithm repeats the following three steps: First, take a step along the vorticity vector to move forward. Second, evaluate the vorticity vector at the new position and construct the normal plane. Third, in this plane, correct the predicted point by setting it to the nearest local pressure minimum. A seed point is found by performing a number of initial steps to establish convergence. This procedure is based on the assumption that the direction of the vorticity vector has little variation compared to the variation of pressure. Under this assumption and for small step sizes, the algorithm yields points where vorticity is approximately parallel to the pressure gradient.

Integration-based methods such as the predictor-corrector method or feature flow fields [47] require a careful placement of seed points and a subsequent removal of duplicates, which we discuss later.

2.4 Meteorological Visualization

With respect to meteorological visualization, our approach is related to the jet-stream core line extraction approach by Kern et al. [24]. They used a local method to extract jet-streams as maximal velocity extremal lines and made the observation that classical local methods commonly produce disjoint and cluttered results. To be more robust they exploited the velocity's directional information by minimizing its magnitude's gradient on an orthogonal plane.

Likewise, our extraction method makes use of directional information. As done by Kern et al. [24] we use a plane perpendicular to the velocity to find local extrema. Kern et al. detected points locally and connected them in a post-process. However, PV banners are extremely thin structures. Due to the highly anisotropic grid spacing, the numerical data contains small variations, which make it difficult for local methods to produce continuous lines in the post-processing step [18]. A simple smoothing would add a user parameter and might merge nearby PV lines, making it therefore not a desirable option. Our method overcomes this issue by using the integration-based predictor-corrector method, which is more robust to variations of PV values along banners, as it exploits flow information of the velocity.

A thorough overview of visualization techniques in meteorology can be found in the survey article by Rautenhaus et al. [34]. The idea of extracting features has been used for multiple 3D flow field characteristics such as topology or vorticity. Post et al. [33] and Heine et al. [20] gave overviews of topology-based visualizations.

3 Requirements

Common practice in meteorology is to visualize 2D slices of potential vorticity [39, 43] as shown in Fig. 1a. However, PV banners are three-dimensional structures and thus their visualization in 3D can support mental model building [34]. In order to learn about the meteorological background and to make the visualization system most useful to our domain scientists, we continuously integrated them into the development process of our visualization system, regularly receiving their feedback and suggestions for improvements. Early on, it became clear that a robust and efficient feature extraction is essential to provide an entry point into the visual exploration and to enable the detailed analysis of PV banners by means of scientific visualizations. Thus, the primary goal of the present work is to identify PV banners from numerical weather prediction data in an automated and robust manner, and to visualize them in a way that benefits a subsequent in-depth meteorological analysis of the atmosphere. Specific requirements have raised the desire for an extraction method in 3D which include:

- **R1:** An appearance of high PV values can occur due to numerous reasons. The approach should allow us to focus on the relevant PV structures, namely the banners starting from mountain ridges. Other structures can be seen in Fig. 1a (north west).
- **R2:** Our domain scientists are interested in an analysis of the PV banner shape, including the geometric properties (length and curvature), the vertical distance to the surface, the change in altitude and the location of the PV banner's origin on the mountains.
- **R3:** Further, an analysis of their dynamic behavior is of high interest, including the lifetime of individual banners. How do they deform over time? When do they start and end? Do they become unstable (i.e., break up into pieces)? Which meteorological situations favor the creation of banners and their decease?
- **R4:** Finally, the system should enable the exploration of the relationship of banners and other meteorological processes such as relative humidity.

Throughout the development process and due to the possibilities provided by the system, our domain scientists raised further questions, digging deeper with us into the spatial and temporal evolution of banners and their interplay with other meteorological processes. In the following, we describe our extraction algorithm and our visualizations.

4 Visual Analysis of Potential Vorticity Banners

4.1 Overview

Our visualization pipeline consists of three steps: the extraction of potential vorticity banners, their spatial and temporal clustering, and finally the interactive visualization using multiple coordinated views. The steps are illustrated in Fig. 3. In Section 4.2, we present the adaption of the predictor-corrector method of Banks and Singer [3] to extract potential vorticity banners from numerical weather prediction data. Section 4.3 describes the spatial and temporal clustering used to remove duplicates and to establish temporal correspondences. Afterwards, Section 4.4 describes the interactive visualizations provided for the visual data analysis, including spatial embeddings in 3D, parallel

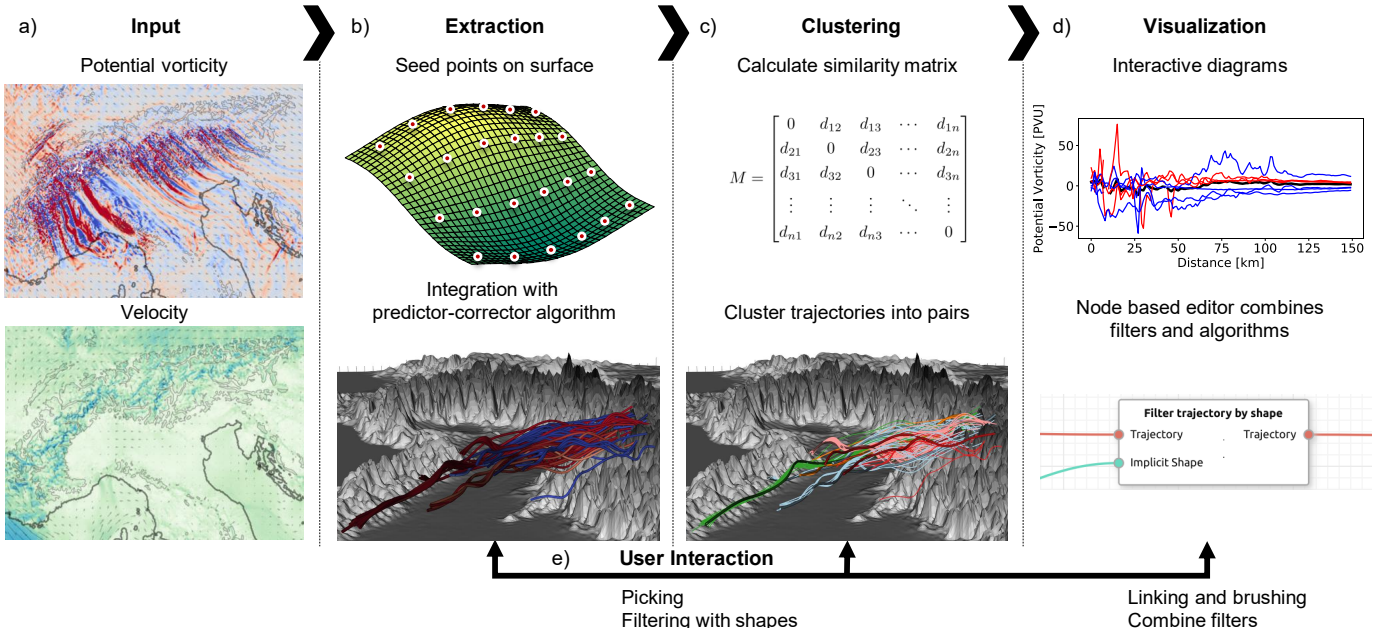

Fig. 3. Method overview. **(a)** The wind velocity and potential vorticity scalar field serve as inputs to our algorithm. **(b)** The PV banner extraction algorithm distributes seed points along the mountain surface and integrates the banners using a predictor-corrector algorithm. **(c)** Clustering similar banners into groups and representatives by constructing a similarity matrix. **(d)** Using multiple linked views, a flexible node-based editor and interactive filtering, we can highlight the desired properties of the banners. **(e)** Users interact with all views by picking as well as linking and brushing.

coordinates, line plots, and a flexible node-based editor for interactive filtering, linking, and brushing.

4.2 Extraction of Potential Vorticity Banners

To capture the geometric shape of potential vorticity banners, we characterize them as extremal lines in the PV scalar field, i.e., as ridge lines or valley lines. Extremal lines are fully captured by the gradient and the Hessian matrix [13, 25]. For meteorological data, however, Kern et al. [24] observed that estimating second-order derivatives for the Hessian suffers from amplification of noise and that smooth interpolation-consistent derivatives are difficult to obtain in practice. Banks and Singer [3] circumvented this issue in the context of vortex core line extraction by taking advantage of the assumption that the direction of the vorticity vector has little variation compared to the variation of pressure. Since PV is an active tracer, i.e., it does not follow the velocity field exactly, the predictor-corrector approach is a good fit to calculate PV extremal lines. In the following, we describe the iterative algorithm, the seeding and the termination criterion.

4.2.1 Predictor-Corrector Algorithm

Starting from a given seed point on a potential vorticity banner, the predictor-corrector algorithm generates extremal lines in the potential vorticity field by repeating the following steps:

- Estimate the velocity direction using the fourth-order Runge-Kutta method [8] at the current point in the potential vorticity banner.
- Step in the velocity direction to predict the location of the next line element.
- Construct a plane that is approximately perpendicular to the velocity and find the closest local PV minimum (maximum) using the method of steepest descent (ascent) [11].
- Correct the position by setting it to the potential vorticity minimum (maximum) in the perpendicular plane.

This algorithm differs from the predictor-corrector method of Banks and Singer [3] only in the chosen scalar and vector field. We do, however, use an optimization to obtain numerically more robust results. We relax the requirement for an exact perpendicular plane to an approximately perpendicular plane that contain the vertical axis. This is because the vertical spacing of the data, which is $\approx 20\,\mathrm{m}$ along the surface, is significantly smaller to the horizontal spacing of 2.2 km in the dataset. Fixing the perpendicular plane to the vertical axis makes the calculation of the gradient numerically more stable and allows us to choose distinct step sizes for the vertical and horizontal direction in the correction step.

The plane is constructed using the velocity $\mathbf{v} = (u, v, w)$ with the three wind components u, v, w defined at grid points at the coordinates x, y, z representing rotated longitude, latitude, and surface aligned model levels, respectively. The resulting plane, visualized in Fig. 4, can be described by following two unit vectors:

$$\mathbf{n} = \frac{(-v, u, 0)}{\|(-v, u, 0)\|}, \quad \mathbf{z} = (0, 0, 1) \tag{4}$$

The closest local extrema can be found using the method of steepest descent (ascent). A local minimum (maximum) is given by:

$$\frac{\partial Q}{\partial \mathbf{n}} = 0 \quad \text{and} \quad \frac{\partial Q}{\partial \mathbf{z}} = 0 \tag{5}$$

We can derive $\frac{\partial Q}{\partial \mathbf{n}} = 0$ by projecting the axis-aligned partial derivatives onto the horizontal unit vector $\mathbf{n}$:

$$\frac{\partial Q}{\partial \mathbf{n}} = \mathbf{n} \cdot \left(\frac{\partial Q}{\partial x}, \frac{\partial Q}{\partial y}, 0 \right) \tag{6}$$

Using the method of steepest descent (ascent) we can approximate the closest local minimum (maximum) by repeatedly correcting the actual predicted point on the plane into the negative (positive) direction of the projected gradient.

The search for the minimum (maximum) in the plane is terminated when the magnitude of the gradient is below a threshold, a maximum number of steps is reached, the change in PV is below a threshold, or if the angle between the predicted and corrected vector is above a specific threshold to prevent the swapping between two neighboring banners.

4.2.2 Seed Points

The integration-based method of the predictor-corrector algorithm requires the placement of seed points. In the atmosphere, line-like

structures of potential vorticity can develop potentially at any point. However, potential vorticity banners originate from orographic peaks[5] and massifs, see Section 2.2 and Fig. 2a. This enables us to take advantage of this property by carefully placing seed points close to the terrain surface. Aside from fulfilling requirement **R1**, i.e., discarding all PV structures that are not PV banners, this allows us to establish the connection between the PV banner and its origin at the mountain (**R2**).

4.2.3 Banner Termination & Filtering

Much like the pressure in a vortex core line, the PV value varies along a PV banner, due to meandering and dissipation, making the threshold-based termination responsive to noise in the data. Thus, we terminate the iterative tracing of a PV banner only when the PV value remains below a user-defined threshold for a certain distance. We defined the distance to be 8.8km which is approximately four horizontal grid cells and the absolute PV threshold to be smaller than 1.0 PVU. The algorithm can extract very short line structures or banners, which can be filtered by the absolute potential vorticity, the accumulated potential vorticity, or a minimal geographic banner length.

4.3 Clustering of Potential Vorticity Banners

The predictor-correct method can lead multiple seeds onto the same potential vorticity banner, since an overabundance of seed points produces a multitude of nearly coincident banner lines. We eliminate the duplicates by taking advantage of the fact that the predictor-corrector method is convergent to the PV core line. Using a distance measure we can find very close lines and classify them as one general PV banner, choosing a representative line. This is required to enable a quantitative analysis of the banners (**R2**), e.g., to compute the average length and the number of banners.

4.3.1 Distance Metric

The distance measure is required to be positive-definitive, symmetric, and it needs to have a low sensitivity to different line lengths. A survey of different line similarity measures complying to these requirements was given by Oeltze et al. [30]. They concluded that the reduced mean of closest point distances (rMCPD)

$$\begin{aligned} d_H(s_i,s_j) &= \min(d_h(s_i,s_j),d_h(s_j,s_i)) \\ \text{with } d_h(s_i,s_j) &= \text{mean}_{p_l\in s_i} \min_{p_k\in s_j} \|p_k - p_l\| \end{aligned} \tag{7}$$

which is an adaptation of the MCPD [10], is especially robust for different line lengths compared with the Hausdorff-Distance [15] and the regular MCPD. In Eq. 7, s_i refers to the i-th line and p_k to the k-th point of the line. The sensitivity of rMCPD is reduced by replacing the outer mean of MCPD by a minimum computation in Eq. (7). For banners with different signs, we set the distance to infinity to avoid the clustering of inherently different banners.

[5]Orographic peaks are local maxima in surface height (mountain tops).

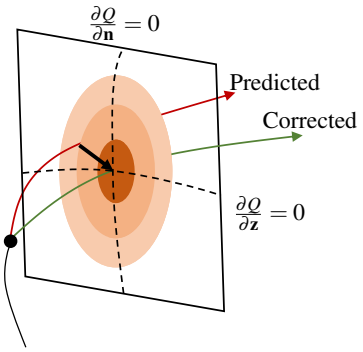

Fig. 4. Illustration of the correction step of the predictor-corrector algorithm, which corrects a predicted point by setting it to the potential vorticity minimum (maximum) using the method of steepest descent (ascent). Projecting the gradient on a plane approximately parallel to the velocity allows us to find the extremum at the intersection of the implicit lines where the gradient of each component is equal to 0.

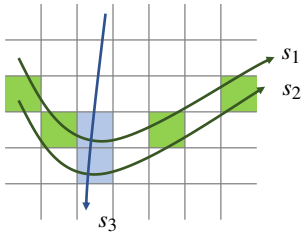

Fig. 5. Cluster algorithm using AHC. The grid represents a spatial data structure. Lines that share a grid cell are compared with each other, e.g., the blue or green shaded cells highlight overlapping line elements in the spatial grid. s_1 and s_2 have a high similarity measure and are clustered together. None of the lines have a high similarity with s_3 and are therefore clustered independently.

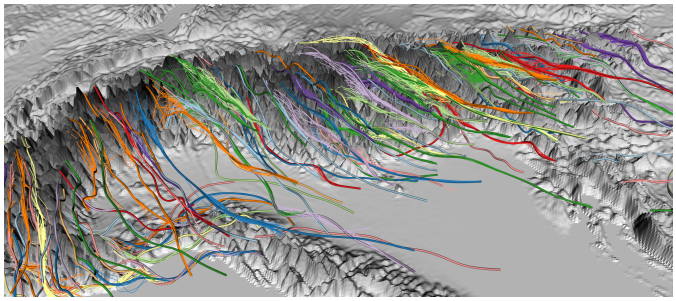

Fig. 6. The PV banners are colored based on their cluster membership. This enables lines to be categorized together that are integrated from different seed points but converged into the same banner. We apply the AHC to group banners and select representative lines.

4.3.2 Spatial Clustering

To group PV banners and to select representative lines, we use the Agglomerative Hierarchical Clustering (AHC) [30]. This algorithm requires a squared symmetric distance matrix M as a measure of cluster proximity, where M contains the pairwise inter-line proximity of all PV banners to each other. We construct the matrix M using the rMCPD distance metric. AHC starts with each line being a cluster and then repeatedly merges the two closest clusters until no cluster is within a user-defined distance threshold. This termination rule has the advantage, compared with other clustering methods such as K-means, that the number of clusters does not have to be known beforehand.

AHC has a high time complexity to compute the matrix M, which requires that all lines need to be compared to each other using the distance metric. To accelerate the computation, we construct a spatial data structure to only compare potentially close enough clusters, (i.e., below the distance threshold) with each other, see Fig. 5. The banners are finally represented by the cluster member with the highest proximity to the other members. Fig. 6 gives an example of the obtained clustering, visualizing each cluster with a different color. Details on the performance of the algorithm can be found later in Section 5.5.

4.3.3 Temporal Clustering

To observe PV banners over time (**R3**) it is necessary to follow specific banners, e.g., to measure their life time. Further, this allows us to raise additional question, e.g., how long does a banner stay stable? How does its curvature, length, or vertical extent behave over time?

We implemented this requirement by clustering over time. As input we take the cluster representatives found with AHC of the time steps t_i and t_{i+1}. By connecting each representative in t_i with the closest representative in t_{i+1} we create a many to 0 relationship through the time steps as visualized in Fig. 7a. If a representative line of t_i has no successor, the algorithm classifies the line as dissolved. If, however, several representatives in t_i connect to the same banner in t_{i+1} we count them as merged together. The same way we can identify newly arising banners if no line in t_i is present for a representative in t_{i+1}. Fig. 7b shows an example of the algorithm where a selection of banners

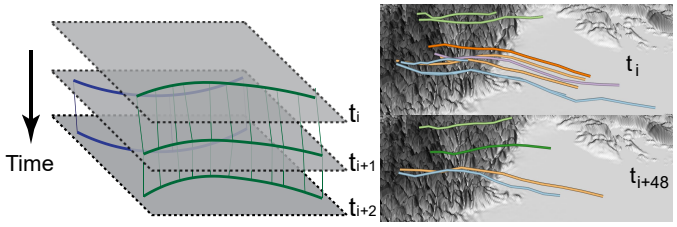

Fig. 7. **(a)** In order to observe the temporal evolution of PV banners, we combine the closest lines between time step t_i and t_{i+1} in a temporal structure. **(b)** Example of the temporal banner tracking, when following a selection of PV banners 8 hours in time (48 time steps). The selection stays stable with a constant color of banners. Some banners dissolve while new others are developed.

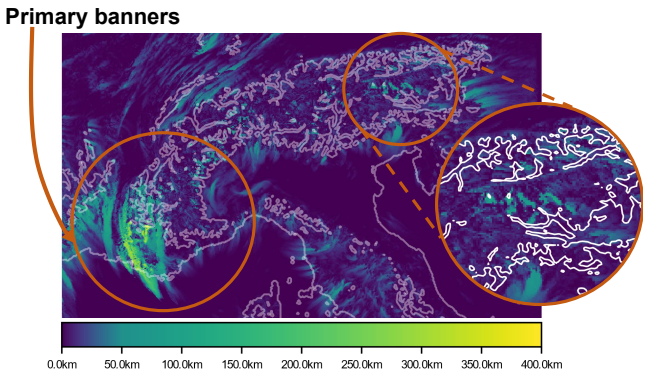

Fig. 8. Time-dependent projection of the PV banners length onto their seed points. Enables perception of geographical important banner seed points. The long banners in the west are part of a primary PV banner in the scale of the whole Alps. Several high peaks (magnified) show an increased banner length compared to their surroundings. 29 January 2010 00:00 to 08:00 UTC.

was observed over time for 24 time steps with a delta time of 10 minutes (4 hours in total). In principle, a number of other feature tracking algorithms are available that could likewise be used, see Saikia and Weinkauf [36]. In order to increase the temporal coherence, we employ a Lagrangian smoothing of the PV field, i.e., the PV value at a certain grid point is calculated by convolving the PV scalar field along a pathline, weighted by a Gaussian filter function, similar to a line integral convolution [9]. The supplemental material contains a video sequence, comparing the temporal clustering with and without Lagrangian smoothing.

4.4 Visualization of Potential Vorticity Banners

Given the PV banners in 3D, we implemented the pathline attributes of Shi et al. [42] to compute a number of derived properties, including line length, accumulated curvature, and life time. Some properties are locally computed per line vertex, others summarize the line behavior globally, such as the average direction, curvature, or the surrounding relative humidity. Our visualization system ties together three interactive views, which include a 3D geospatial view, multi-variate information visualizations, and a time-series view. Each view gives a different perspective onto the data and allows for real-time exploration. Furthermore, each view is linked so that selections and interactions in one view simultaneously affect the other as visualized in Fig. 10a and 10b. In the following, we discuss the three views and our node-based visualization and filtering system in more detail.

4.4.1 Geospatial View

In the 3D view, PV banners are visualized as colored tubes with the topography being rendered in the background to provide a geospatial context. In order to enable the analysis of correlations among line attributes (**R2**) and with meteorological attributes (**R4**), properties can be mapped to the radius, color, and opacity of the tubes. Embedded into the 3D space, the viewer obtains an impression of the general PV banner shape and their alignment with wind vectors.

Displaying the full set of banners may result in visual clutter. We therefore provide two approaches to reduce the amount of data. First, the user can interactively place regions-of-interest to select individual banners, as shown in Fig. 10c. The banners are then highlighted, whereas the remaining lines are desaturated, providing focus and context, as done in Fig. 7b. Second, since all relevant PV banners were released from the mountains (**R1**), line properties can be directly mapped to the seed point. This way, a scalar field is obtained that is directly embedded on the mountain surface, which is a 2D manifold in the 3D space. Fig. 8 shows a time-dependent projection of the average banner length onto the surface.

To study correlations with meteorological attributes (**R4**), e.g., updraft wind, relative humidity, or potential vorticity itself, a 2D plane can be placed in the scene. For a selected PV banner, the upright-oriented plane can be moved interactively along the line. With this, atmospheric parameters can be directly visualized in the vicinity of the banner. The plane can be aligned perpendicular to the line, tangential to it, or in the horizontal layer. Furthermore, glyphs can be placed on the plane for instance to show the direction of three-dimensional vectors, e.g., velocity, vorticity, or gradients of scalar values, as done in Fig. 2b.

4.4.2 Multi-Variate View

In order to explore the multi-variate attributes (**R2**, **R4**), common information visualization techniques are used to discover relevant correlations, interesting feature combinations, or general properties of the data. Our application supports 2D scatter plots, parallel coordinates and histograms, as shown for instance in Fig. 10a or Fig. 12. We employ linking and brushing, i.e., users can select certain properties in one view which are then propagated onto all linked views by an appropriate focus and context switch. This combination of views makes it possible to analyze a wide variety of scalar quantities.

4.4.3 Time-Series View

While the previously presented visualization techniques are effective for comparing trends between variables as well as spatial differences throughout the domain, they are not effective for the visualization of trends over time (**R3**). For this, we implemented a separate time-series view that displays the temporal properties of selected banners in interactive line plots, as shown later in Fig. 13. We rely on the temporal clustering from Section 4.3.3 to establish the temporal correspondence, which in turn allows us to infer information about a banner's life cycle. The different lines through time can be interactively compared.

4.4.4 Node-based Editor

To allow a high degree of flexibility while hiding the complexity of the underlying algorithms from the user a data flow programming paradigm [23] was implemented. Further information on the design choices is discussed in Section 5.3. Data flow programming allows the definition of a program as a directed graph where the data flows between operations. Explicitly defined inputs and outputs connect operations that are executed as soon as all of their inputs become valid. The resulting user interface is shown in Fig. 9, allowing the creation of seeding structures, visualization methods and visualization parameters.

5 Results

We demonstrate the extraction method and the developed framework by analyzing the output of two real-case simulations. In the remainder of this section, we provide an overview of the climate simulation and analyze specific aspects of the data. We conclude the presented work by giving an insight into the development process, the design lessons learned, a performance analysis, and finally a summary and conclusion.

5.1 Data

Our study utilizes data from the COSMO (Consortium for Small-scale Modeling) weather and climate model, which is a nonhydrostatic limited-area model that solves the fully compressible governing equations using finite difference methods on a structured grid [45]. The data

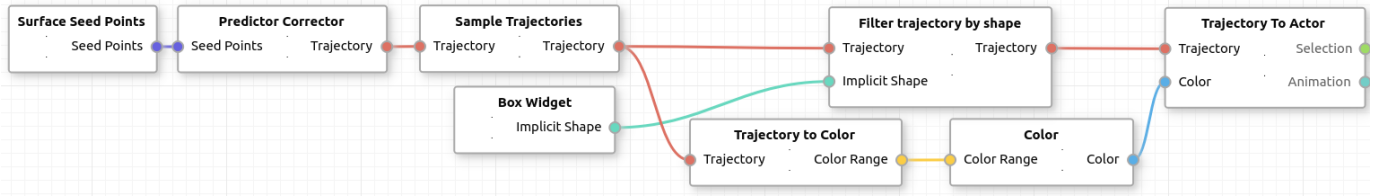

Fig. 9. Data flow programming enables a high degree of flexibility by combining operators through connections while hiding the underlying algorithmic complexity. This specific example samples seed points along the surface, integrates the banners using the predictor corrector algorithm, filters the banners that are within a user defined box, and shows them in the view using the depicted color maps.

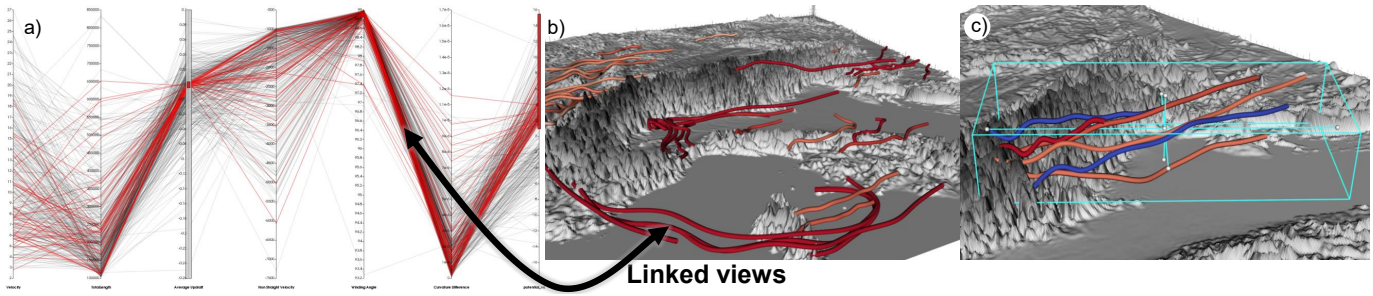

Fig. 10. **(a)** Parallel Coordinates Diagram. Selection of positive PV banners with low updraft which automatically updates all other views. **(b)** Updated view according to selection in (a). **(c)** Limit selection by placing shapes in the scene. E.g., box shape that only shows banners within.

is computed using a refactored version of COSMO using GPU accelerators [16] that allows the refinement of the model resolution to the kilometer scale on continental scales. The advantage of high-resolution km-scale models is a better representation of the underlying orography and the associated flow, and it enables an explicit representation of convection (i.e., thunderstorms and rain showers, vertical circulation – updrafts and downdrafts) that conventional weather and climate models are not suited to resolve without parameterization [2, 27].

The model is discretized on a rotated latitude-longitude grid using terrain-following altitude coordinates. The configuration has a convection-resolving horizontal grid spacing of 2.2 km and $1536 \times 1536 \times 60$ grid points with a time step of 20 seconds. The vertical direction is discretized using 60 stretched model levels from the surface to the model top at 23.5 km. The respective layer thickness widens from 20 m at the surface to 1.2 km near the model top. The necessary initial and boundary condition for the model are derived from the European Centre for Medium-Range Weather Forecasts (ECMWF) ERA-Interim reanalysis [12] and are updated every 6 h. We followed the model setup defined in Leutwyler et al. [28].

From the simulation domain, a subset of $500 \times 500 \times 60$ grid cells over the Swiss Alps was extracted to analyze the potential vorticity banners over the Alps. We simulated two week-long cases starting at April 10, 2000 and January 27, 2010, and output the data every 10 minutes. In total, the numerical simulation data accumulated to 3 TB.

5.2 Analysis

By applying the presented visualization methods we obtain a deeper understanding of the PV banners and their meteorological surroundings. We present our findings by first analyzing distinct banners, then investigate their structure over the Alps and the downstream topography, and finally we observe their life cycle in the temporal dimension.

5.2.1 Extraction of distinct Potential Vorticity Banners

The meteorological conditions between the 28 and 29 January 2010 were favorable for the development of PV banners around the Alps due to the strong wind flowing from north to south above the full extent of the Alps. An overview of the 28 January 2010 12:00 UTC is given in Fig. 1 where the PV banners extend several hundred km downstream.

We extracted a subset of PV banners (see Fig. 13a), originating from neighboring mountain peaks in the west of the Alps where the topography downstream enables the banners to extend undisturbed. The extracted banners confirm known patterns, namely PV values of

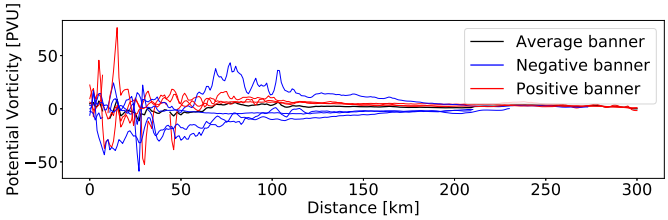

Fig. 11. PV value along the extracted core lines. The absolute PV value declines with the length of the banner. Typically the neighboring PV banners with anomalously positive (red) and negative (blue) signs show similar trends along their length. The mean is shown as a black line.

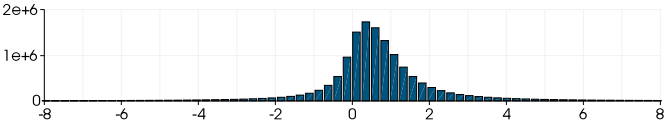

Fig. 12. Distribution of PV in the model's atmosphere. Cells of constant volume are sampled in the altitude range between 0 km and 6 km above sea level. The mean of the normally distributed PV values is slightly shifted to the positive side, which was expected by the meteorologists.

anomalously positive and negative sign and PV values declining with the length of the banners. Fig. 11 illustrates the PV values along the extracted core lines. The neighboring PV banners, which typically differ in their sign, show a similar decay of PV along their length. This results in a linear structure of the mean values of the extracted PV banners. Comparing this with the PV distribution of the model's atmosphere (see Fig. 12) we observe that the PV values at the banners source deviate significantly from the mean.

After the flow detaches from the mountain peaks, PV banners show a wave-like vertical displacement which Fig. 13c outlines by the fluctuating altitude changes of the PV banners. It turns out that this pattern can also be observed in the vertical component (Fig. 13b) of the velocity. These motions are due to atmospheric gravity (buoyancy) waves, which generate when a stably stratified fluid is forced to flow over a topographic barrier, thereby producing vertical motions. Depending on the upstream vertical profiles of velocity and density, the wave energy may be trapped and the flow response then exhibits quasi-stationary waves with a well-defined horizontal wave length. The occurrence of such waves in flow past topography is common, but to our knowledge

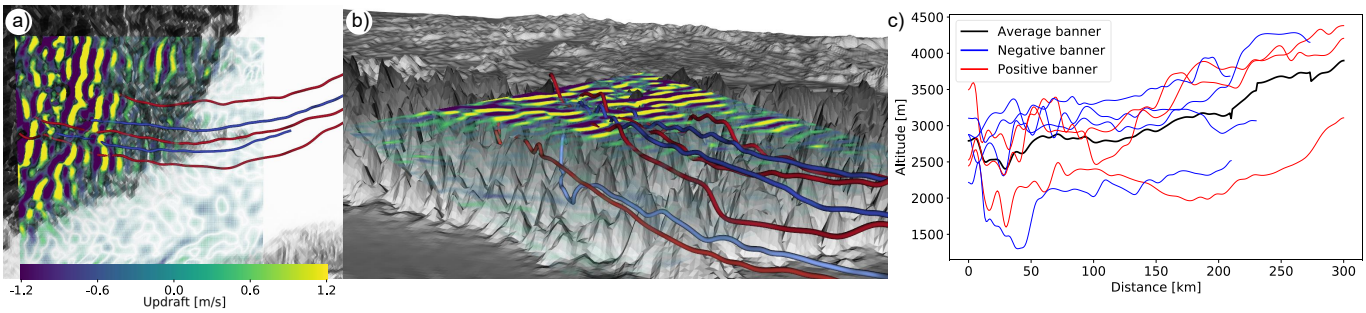

Fig. 13. **(a)** Selected PV banners are shown to analyze their spatial extent. **(b)** A visualization of a horizontal cross section of the vertical wind component at fixed altitude along the PV banner is shown. The wavelike patterns in the flow direction (from left to right) is associated with atmospheric gravity (or buoyancy) waves and is responsible for the altitude changes of PV banners. **(c)** A plot of the altitude of the PV banners along their full extent is depicted. The banners show an undulating pattern in the altitude change close to their source.

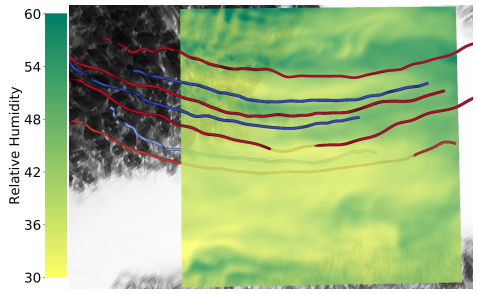

Fig. 14. Relative humidity extracted as a horizontal cross section around the PV banners on 2500m above sea level. A correlation between the PV banners and relative humidity values is visible. This highlights that PV banners separate air masses of alternating high and low humidity.

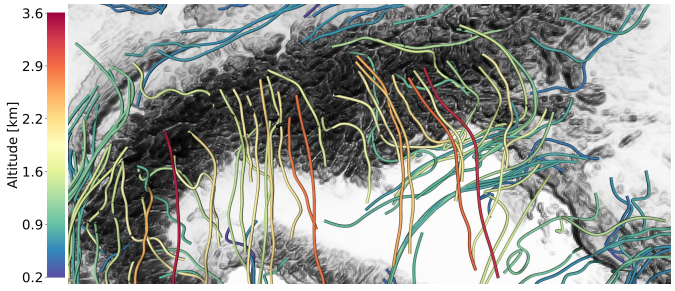

Fig. 15. 27 January 2010 20:10 UTC. PV banners color-mapped by altitude. Banners at different altitudes exhibit different directions and may cross each other. Comprehending these crossings is straightforward in our 3D visualization, but difficult to detect in standard horizontal displays.

their interaction with PV banners has not been noted previously.

The extraction of PV banners facilitates the analysis of their relationship with the atmospheric environment. In Fig. 14, a horizontal cross section of relative humidity gives a specific example where a correlation of PV banners and other meteorological variables can be identified. Relative humidity is not fully conserved by atmospheric transport, but it nevertheless serves as a tracer of air mass. The PV banners separate air masses of different origin and thus different relative humidity. Some have passed the Alps and carry along comparatively high humidity associated with condensation processes to the north of the Alps, others origin from low-levels to the south of the Alps and exhibit comparatively low humidity. However, these relationships are complicated as descending air masses will dry due to adiabatic warming.

The ability to map a multitude of meteorological parameters via color onto the extracted banners or onto plane cross sections provides the user insight into atmospheric processes along the banners that could not be inferred from the conventional 2D approaches.

5.2.2 Structure of PV Banners over the Alps

The development of PV banners at a specific mountain peak depends on several criteria. One specific prerequisite for the development of elongated lines is that the model's topography downstream is sufficiently smooth. Their extension direction is highly dependent on the wind direction. Because of this a north- or south-bound flow is favorable for the development of PV banners in the European Alps since the PV banners can develop on the whole mountain range.

PV banners can develop in different directions over several altitude levels. Fig. 15 shows PV banners color-mapped by their altitude. Compared with a conventional 2D visualization, the 3D visualization allows an analyst to easily perceive the vertical staggering of the banners. This facilitates the identification of crossings between banners at different altitudes in a straightforward way. The different directions of the banners are due to different wind directions depending on the altitude. The resulting crossings of banners are consistent with meteorological expectations, but have to our knowledge not been shown previously.

Besides PV banners, it is possible to have a PV accumulation in the atmosphere created by processes other than flow detachment around mountains or their peaks. One specific example can be observed in the north west of Fig. 1 (c) where the accumulation is caused by a meteorological front. Because of this, it is required that our extraction algorithm can differentiate robustly between PV banners, i.e., PV accumulations that are created from flow detachment, and other PV accumulations.

5.2.3 Time-dependent Analysis

The life cycle of PV banners starts with their creation and ends with their decay. Typically they have a life time of several hours. Responsible for their decay can be a multitude of meteorological processes. Mainly they are: wind speed at source drops, the wind downstream disturbs their development or the wind direction changes over rough topography which prohibits PV banners to develop. When they reach their end of life they typically reduce their length and vanish or they decay into parts which are advected downstream by the wind. For example, Fig. 16 shows the decay of a group of PV banners over a time period of 5 hours. This decay was caused by the wind downstream, which disturbed the banner development. The banners start to deviate from their course and their tails detach from their sources.

Fig. 8 shows the temporal accumulation of the PV banner length projected onto the surface for a time period of 8 hours. This allows the user to get good temporal overviews of the dataset. In the mountain range on the west, we see the source points of long primary banners, which extend over the whole mountain range. Furthermore, several high peaks show increased lengths compared to their surroundings, which further emphasizes the flow detachment at the mountain peaks.

5.3 Development Process & Design Lessons

We carefully designed the application in a tight feedback loop with our collaborators. This allowed us to develop the system through repeated cycles (iterative) and in small portions at a time (incremental), allowing the developers to take advantage of what was learned during the development of earlier versions of the tool.

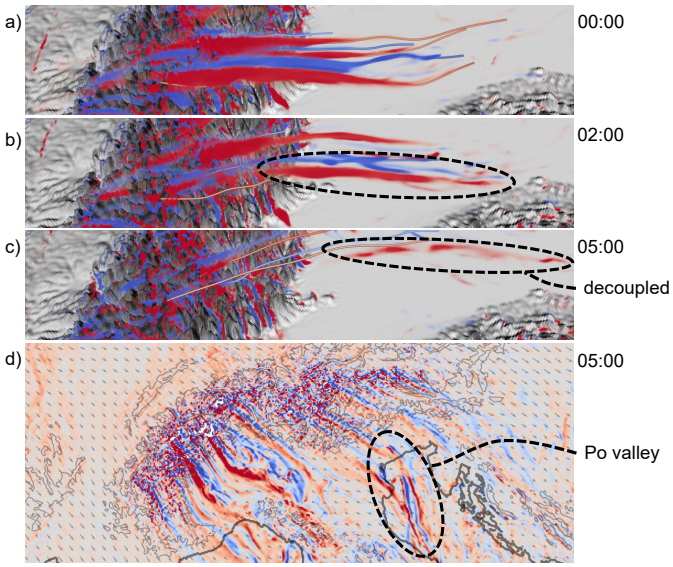

Fig. 16. 29 January 2010 from 00:00 to 05:00 UTC. End of lifetime sequence of PV banners which are rendered as volumes with the corresponding core lines as geometrical lines. **(a)** The wind flows from north (left) to south (right). The wind direction in the Po valley changes eastwards which is responsible for the eastward bend in their end. **(b)** The PV banner start to decouple from the mountains source. **(c)** The decoupled PV banners are advected with the wind flowing over the Alps. **(d)** A horizontal cross section of the PV banners on 3000m above sea level emphasizes the decoupling of the PV banners.

The iterative process involved a requirement analysis, which defined the project goals. In an exploration process, a first prototype was developed which enabled the domain specialists to get first insights of the advantages and additional possibilities provided by 3D visualizations of climate data. This allowed the team to define the necessary visualization techniques and to refine the requirements. The parallel development of the interactive visualizations enabled an agile change process to collectively refine the requirements and adapt the application.

A specific example where this agile reaction on changes was required is the implementation of the data flow programming model. The close cooperation between the domain scientists and developers revealed that the prototyped application did not enable the degree of freedom to combine different algorithms and visualization techniques, as desired. The user interfaces were too complicated to allow complex and flexible filtering. This led us to research other possibilities to provide the end user a better access to the underlying algorithms and data. The final decision to satisfy this requirement was to implement the node-based data flow programming model.

5.4 Development Environment

The PV banner extraction is implemented in C++ using the Visualization Toolkit (VTK) [40]. The graphical user interface was designed using the cross platform development kit QT and the node-based user interface was implemented using QT Node Editor [32].

5.5 Performance

This section reports on the performance of our approach. The focus is on the computation time, since the memory consumption to store PV banners is negligible compared to the simulation data size. Our method depends on the precalculation of the potential vorticity, a scalar value which is not necessarily available in a meteorological dataset. The computation time to extract banners is inherently dependent on the number of seed points which determines the number of lines to be integrated. The PV line computation is parallelized, since the extraction of each banner candidate is independent. All timings were taken on a workstation with an Intel Core i7 8700 processor with 3.2 GHz $\times$ 6 cores, 16 GB RAM and a NVIDIA GeForce GTX 1050TI.

# Seedpoints	200,000	50,000	10,000
# Banner	13,764	3,430	519
# Cluster	996	617	252
Integration time	9,300ms	2,300ms	352 ms
Cluster time	880ms	100ms	10ms
Visualization time	10ms	3ms	1ms
Precomputation of PV	3,700ms	(independent of seedpoints)	

Table 1. The timings were measured on a grid with $500 \times 500 \times 60$ resolution, based on the node graph earlier shown in Fig. 9.

The most time consuming part was the gradient calculation and the gradient descent method used to correct the banners, which is particularly expensive due to the conversion of the surface aligned model levels to meters. The method enables a high scalability to larger datasets. Limits could be pushed further by employing a GPU integration or by distributing the work on several machines.

6 Summary & Discussion

We presented a method to extract potential vorticity banners from regional numerical weather prediction data. Our method is independent of the model, and might also be used with other high-resolution models such as NICAM or ICON. The method is based on the integration-based predictor-corrector [3] algorithm to find extremal lines in the PV data. Our method is able to robustly extract the extremal lines over long distances and through noisy scalar fields. We place the seed points above the terrain to filter out PV accumulations that are not based on orographic flow splitting. Using AHC we are able to combine different banners that converge into the same banner structure. We implemented a workflow that enables the user to interactively identify PV banners and to track them through time. To facilitate the analysis, we provide several visualization techniques such as line visualizations and information visualizations supporting linking and brushing. We demonstrated the framework on the analysis of PV banners in two numerical data sets, highlighting the value of our method.

In close collaboration with the domain scientists, we designed an application that fulfills the given requirements to facilitate further research on PV banners. The time needed to compute the banners is within seconds to a few minutes and the analysis of the data can be done at interactive frame rates. Our approach makes the data more accessible, since it becomes easier to interpret the spatial structure of the extracted line features, compared to the currently used 2D visualizations. The method is able to remove visual clutter and enables the observation of PV banners over time. This is of crucial importance to understand the spatial structure of PV banners, to explore the relationship between the banners and their environment and to study the life cycle of PV banners. In particular, we shed light onto two inherently three-dimensional processes that have previously not been visualized: the vertical crossing of potential vorticity banners in different altitude levels, and their vertical waviness in the lee of the mountains.

A limitation of our approach is that it produces an overabundance of seed points which have to be clustered to representative banners. The overabundance of seed points results in additional computational effort and additional filtering is necessary in a post-processing step. Future work might include the extraction of tubes around core lines which would allow further insight into the surroundings of PV banners, and it would be interesting to investigate topological smoothing methods [48] to stabilize the extremal line extraction.

Acknowledgments

This work was supported by the Swiss National Science Foundation (SNSF) Ambizione grant no. PZ00P2_180114. The atmospheric model simulations have been supported by the Swiss National Science Foundation under Sinergia grant CRSII2_154486/1 crCLIM. In addition, we acknowledge PRACE for awarding us access to Piz Daint at CSCS (Switzerland) where the simulations are integrated.

REFERENCES

[1] U. Aebischer and C. Schär. Low-Level Potential Vorticity and Cyclogenesis to the Lee of the Alps. *Journal of the Atmospheric Sciences*, 55(2):186–207, 1998. doi: 10.1175/1520-0469(1998)055<0186:LLPVAC>2.0.CO;2

[2] N. Ban, J. Schmidli, and C. Schär. Heavy precipitation in a changing climate: Does shortterm summer precipitation increase faster? *Geophysical Research Letters*, 42(4):1165–1172, 2015. doi: 10.1002/2014GL062588

[3] D. C. Banks and B. A. Singer. Vortex tubes in turbulent flows: identification, representation, reconstruction. *IEEE Conference on Visualization*, pp. 132–139, 1994. doi: 10.1109/VISUAL.1994.346327

[4] D. A. Bennetts and B. J. Hoskins. Conditional symmetric instability a possible explanation for frontal rainbands. *Quarterly Journal of the Royal Meteorological Society*, 105(446):945–962, 1979. doi: 10.1002/qj.49710544615

[5] R. Benoit, C. Schär, P. Binder, S. Chamberland, H. Davies, M. Desgagné, C. Girard, C. Keil, N. Kouwen, D. Lüthi, D. Maric, E. Müller, P. Pellerin, J. Schmidli, F. Schubiger, C. Schwierz, M. Sprenger, A. Walser, S. Willemse, W. Yu, and E. Zala. The Real-Time Ultrafinescale Forecast Support during the Special Observing Period of the MAP. *Bulletin of the American Meteorological Society*, 83(1):85–109, 2002. doi: 10.1175/1520-0477(2002)083<0085:trtufs>2.3.co;2

[6] M. Boettcher and H. Wernli. Life Cycle Study of a Diabatic Rossby Wave as a Precursor to Rapid Cyclogenesis in the North AtlanticDynamics and Forecast Performance. *Monthly Weather Review*, 139(6):1861–1878, 2011. doi: 10.1175/2011mwr3504.1

[7] P. Bougeault, P. Binder, A. Buzzi, R. Dirks, R. Houze, J. Kuettner, R. B. Smith, R. Steinacker, and H. VoIkert. The MAP special observing period. *Bulletin of the American Meteorological Society*, 82(3):433–462, 2001.

[8] C. Runge. Ueber die numerische Auflösung von Differentialgleichungen. *Mathematische Annalen*, 46(2):167–178, 1895.

[9] B. Cabral and L. C. Leedom. Imaging vector fields using line integral convolution. Technical report, Lawrence Livermore National Lab., CA (United States), 1993. doi: 10.1145/166117.166151

[10] I. Corouge, S. Gouttard, and G. Gerig. Towards a shape model of white matter fiber bundles using diffusion tensor MRI. *2004 2nd IEEE International Symposium on Biomedical Imaging: Nano to Macro (IEEE Cat No. 04EX821)*, pp. 344–347, 2004. doi: 10.1109/isbi.2004.1398545

[11] P. Debye. Näherungsformeln für die Zylinderfunktionen für große Werte des Arguments und unbeschränkt veränderliche Werte des Index. *Mathematische Annalen*, 67(4):535–558, 1909.

[12] D. P. Dee, S. M. Uppala, A. J. Simmons, P. Berrisford, P. Poli, S. Kobayashi, U. Andrae, M. A. Balmaseda, G. Balsamo, P. Bauer, P. Bechtold, A. C. M. Beljaars, L. van de Berg, J. Bidlot, N. Bormann, C. Delsol, R. Dragani, M. Fuentes, A. J. Geer, L. Haimberger, S. B. Healy, H. Hersbach, E. V. Hólm, L. Isaksen, P. Kallberg, M. Köhler, M. Matricardi, A. P. McNally, B. M. Monge-Sanz, J. Morcrette, B. K. Park, C. Peubey, P. de Rosnay, C. Tavolato, J. Thépaut, and F. Vitart. The ERA-Interim reanalysis: configuration and performance of the data assimilation system. *Quarterly Journal of the Royal Meteorological Society*, 137(656):553–597, 2011.

[13] D. Eberly. *Ridges in image and data analysis*, vol. 7. Springer Science & Business Media, 2012. doi: 10.1007/978-94-015-8765-5

[14] H. Ertel. Ein neuer hydrodynamischer Erhaltungssatz. *Naturwissenschaften*, (3):543–544, 1942. doi: 10.1007/BF01475602

[15] F. Exploration, H. Theisel, and C. Ro. Streamline Embedding for 3D Vector. *IEEE Transactions on Visualization and Computer Graphics*, 18(3):407–420, 2012. doi: 10.1109/TVCG.2011.78

[16] O. Fuhrer, C. Osuna, X. Lapillonne, T. Gysi, M. Bianco, A. Arteaga, and T. C. Schulthess. Towards a performance portable, architecture agnostic implementation strategy for weather and climate models. *Supercomputing Frontiers and Innovations*, 1(1):44–61, 2014. doi: 10.14529/jsfi140103

[17] T. Günther, M. Schulze, and H. Theisel. Rotation Invariant Vortices for Flow Visualization. *IEEE Transactions on Visualization and Computer Graphics*, 22(1):817–826, 2016. doi: 10.1109/TVCG.2015.2467200

[18] T. Günther and H. Theisel. The State of the Art in Vortex Extraction. *Computer Graphics Forum*, 37(6):149–173, 2018. doi: 10.1111/cgf.13319

[19] H.-C. Hege, H. Theisel, T. Weinkauf, and J. Sahner. Cores of Swirling Particle Motion in Unsteady Flows. *IEEE Transactions on Visualization and Computer Graphics*, 13(6):1759–1766, 2007. doi: 10.1109/TVCG.2007.70545

[20] C. Heine, H. Leitte, M. Hlawitschka, F. Iuricich, L. De Floriani, G. Scheuermann, H. Hagen, and C. Garth. A survey of topology-based methods in visualization. *Computer Graphics Forum*, 35(3):643–667, 2016. doi: 10.1111/cgf.12933

[21] B. J. Hoskins. The role of potential vorticity in symmetric stability and instability. *Quarterly Journal of the Royal Meteorological Society*, 69(300):155–162, 1974. doi: 10.1002/qj.49710042520

[22] B. J. Hoskins, M. E. McIntyre, and A. W. Robertson. On the use and significance of isentropic potential vorticity maps. *Quarterly Journal of the Royal Meteorological Society*, 111(6):877–946, 1985. doi: 10.1002/qj.49711147002

[23] W. M. Johnston, J. R. P. Hanna, and R. J. Millar. Advances in dataflow programming languages. *ACM Computing Surveys*, 36(1):1–34, 2004. doi: 10.1145/1013208.1013209

[24] M. Kern, T. Hewson, F. Sadlo, R. Westermann, and M. Rautenhaus. Robust Detection and Visualization of Jet-Stream Core Lines in Atmospheric Flow. *IEEE Transactions on Visualization and Computer Graphics*, 24(1):893–902, 2018. doi: 10.1109/TVCG.2017.2743989

[25] G. Kindlmann, C. Chiw, T. Huynh, A. Gyulassy, J. Reppy, and P.-T. Bremer. Rendering and extracting extremal features in 3D fields. *Computer Graphics Forum (Proc. EuroVis)*, 37(3):525–536, 2018. doi: 10.1111/cgf.13439

[26] N. Kljun, M. Sprenger, and C. Schär. Frontal modification and lee cyclogenesis in the alps: A case study using the alpex reanalysis data set. *Meteorology and Atmospheric Physics*, 78(1-2):89–105, 2001. doi: 10.1007/s007030170008

[27] D. Leutwyler, O. Fuhrer, X. Lapillonne, D. Lüthi, and C. Schär. Towards European-scale convection-resolving climate simulations with GPUs: A study with COSMO 4.19. *Geoscientific Model Development*, 9(9):3393–3412, 2016. doi: 10.5194/gmd-9-3393-2016

[28] D. Leutwyler, D. Lüthi, N. Ban, O. Fuhrer, and C. Schär. Evaluation of the convection-resolving climate modeling approach on continental scales. *Journal of Geophysical Research*, 122(10):5237–5258, 2017. doi: 10.1002/2016JD026013

[29] H. Miura and S. Kida. Identification of Tubular Vortices in Turbulence. *Journal of the Physical Society of Japan*, 66(5):1331–1334, 1997. doi: 10.1143/JPSJ.66.1331

[30] S. Oeltze, D. J. Lehmann, A. Kuhn, G. Janiga, H. Theisel, and B. Preim. Blood flow clustering and applications invirtual stenting of intracranial aneurysms. *IEEE Transactions on Visualization and Computer Graphics*, 20(5):686–701, 2014. doi: 10.1109/TVCG.2013.2297914

[31] R. Peikert and M. Roth. The "Parallel Vectors" operator-a vector field visualization primitive. *Proceedings Visualization '99 (Cat. No.99CB37067)*, pp. 263–532, 1999. doi: 10.1109/VISUAL.1999.809896

[32] D. Pinaev. Qt5 node editor. `https://github.com/paceholder/nodeeditor`, 2017.

[33] F. H. Post, B. Vrolijk, H. Hauser, R. S. Laramee, and H. Doleisch. The State of the Art in Flow Visualisation :. *Computer Graphics Forum*, 22(4):775–792, 2003. doi: 10.1111/j.1467-8659.2003.00723.x

[34] M. Rautenhaus, M. Bottinger, S. Siemen, R. Hoffman, R. M. Kirby, M. Mirzargar, N. Rober, and R. Westermann. Visualization in Meteorology - A Survey of Techniques and Tools for Data Analysis Tasks. *IEEE Transactions on Visualization and Computer Graphics*, 24(12):3268–3296, 2018. doi: 10.1109/TVCG.2017.2779501

[35] J. Sahner, T. Weinkauf, N. Teuber, and H. C. Hege. Vortex and strain skeletons in eulerian and Lagrangian frames. *IEEE Transactions on Visualization and Computer Graphics*, 13(5):980–989, 2007. doi: 10.1109/TVCG.2007.1053

[36] H. Saikia and T. Weinkauf. Global feature tracking and similarity estimation in time-dependent scalar fields. *Computer Graphics Forum (Proc. EuroVis)*, 35(3):1–11, 2017. doi: 10.1111/cgf.13163

[37] C. Schär, A. Arteaga, C. C. N. Ban, S. di Girolamo, O. Fuhrer, T. H. L. Hentgen, X. Lapillonne, D. Leutwyler, K. Osterried, D. Panosetti, S. Rüdisühli, L. Schlemmer, T. Schulthess, M. Sprenger, S. Ubbiali, and H. Wernli. Kilometer-scale climate models: Prospects and challenges. *Bulletin of the American Meteorological Society*, 2019. in revision.

[38] C. Schär, G. Kwasniewski, H. Vogt, T. Chadha, T. C. Schulthess, X. Lapillonne, C. Osuna, D. Lüthi, O. Fuhrer, D. Leutwyler, and T. Hoefler. Near-global climate simulation at 1 km resolution: establishing a performance baseline on 4888 GPUs with COSMO 5.0. *Geoscientific Model Development Discussions*, pp. 1–27, 2017. doi: 10.5194/gmd-2017-230

[39] C. Schär, M. Sprenger, D. Lüthi, Q. Jiang, R. B. Smith, and R. Benoit. Structure and dynamics of an Alpine potential-vorticity banner. *Quarterly Journal of the Royal Meteorological Society*, 129(588 PART B):825–855,

2003. doi: 10.1256/qj.02.47

[40] W. Schroeder, K. Martin, and B. Lorensen. *The Visualization Toolkit (4th ed.)*. 2006.

[41] R. S. Schumacher, D. M. Schultz, and J. A. Knox. Convective snowbands downstream of the rocky mountains in an environment with conditional, dry symmetric, and inertial instabilities. *Monthly Weather Review*, 138(12):4416–4438, 2010. doi: 10.1175/2010MWR3334.1

[42] K. Shi, H. Theisel, H. Hauser, and T. Weinkauf. Path Line Attributes - an Information Visualization Approach to Analyzing the Dynamic Behavior of 3D Time-Dependent Flow Fields. *TopoInvis*, 2007. doi: 10.1007/978-3-540-88606-8_6

[43] S. K. Siedersleben and A. Gohm. The Missing Link between Terrain-Induced Potential Vorticity Banners and Banded Convection. *Monthly Weather Review*, 144(11):4063–4080, 2016. doi: 10.1175/MWR-D-16-0042.1

[44] M. Sprenger, G. Fragkoulidis, H. Binder, M. Croci-Maspoli, P. Graf, C. Grams, P. Knippertz, E. Madonna, S. Schemm, B. Škerlak, and H. Wernli. Global Climatologies of Eulerian and Lagrangian Flow Features based on ERA-Interim. *Bulletin of the American Meteorological Society*, 98(8):1739–1748, 2017. doi: 10.1175/bams-d-15-00299.1

[45] J. Steppeler, G. Doms, U. Schättler, H. W. Bitzer, A. Gassmann, U. Damrath, and G. Gregoric. Meso-gamma scale forecasts using the nonhydrostatic model lm. *Meteorology and Atmospheric Physics*, 82(1):75–96, 2003. doi: 10.1007/s00703-001-0592-9

[46] R. C. Strawn, D. N. Kenwright, and J. Ahmad. Computer Visualization of Vortex Wake Systems. *AIAA Journal*, 37(4):511–512, 1999. doi: 10.2514/2.744

[47] H. Theisel, T. Weinkauf, H. C. Hege, and H. P. Seidel. Saddle Connectors - An Approach to Visualizing the Topological Skeleton of Complex 3D Vector Fields. *Proceedings of the IEEE Visualization Conference*, pp. 225–232, 2003. doi: 10.1109/VISUAL.2003.1250376

[48] T. Weinkauf, Y. Gingold, and O. Sorkine. Topology-based smoothing of 2d scalar fields with c1-continuity. *Computer Graphics Forum*, 29(3):1221–1230, 2010. doi: 10.1111/j.1467-8659.2009.01702.x